Phase separation and crystallization in the Zr41.2–Ti13.8–Cu12.5–Ni10–Be22.5 bulk metallic glass determined by physical measurements and electron microscopy

Jean-marc Pelletier, Bertrand van de Moortele

Phase separation and crystallization in the $Zr_{41.2}$–$Ti_{13.8}$–$Cu_{12.5}$–Ni_{10}–$Be_{22.5}$ bulk metallic glass determined by physical measurements and electron microscopy

J.M. Pelletier *, B. Van de Moortèle

GEMPPM, INSA Lyon, bat. Blaise Pascal, 69621 Villeurbanne cedex, France

Phase separation and crystallization processes of bulk amorphous $Zr_{41.2}$–$Ti_{13.8}$–$Cu_{12.5}$–Ni_{10}–$Be_{22.5}$ (Vitreloy 1) are reported. In addition to classical differential scanning calorimetry and X-ray diffraction experiments, thermoelectric power (TEP) measurements, mechanical spectroscopy and high resolution transmission electron microscopy (HR-TEM) observations are performed. During annealing in the supercooled liquid region both reversible and irreversible microstructure evolutions are observed before the onset of crystallization, as indicated by a TEP variation, which can be positive or negative, depending on annealing conditions. Once the crystallization process is started, size and volume fraction of nanocrystallized particles increase. The isolated nanocrystals increase the elastic features in the glass temperature region, but the main viscoelastic relaxation is still observed, indicating therefore that the crystalline phase embedded in the decomposed amorphous matrix does not form a continuous network of rigid particles. Both phase separation and crystallization processes are discussed on the basis of microstructure observations, physical and mechanical measurements.

1. Introduction

Among multicomponent bulk metallic glasses forming alloy systems, the $Zr_{41.2}$–$Ti_{13.8}$–$Cu_{12.5}$–Ni_{10}–$Be_{22.5}$ (Vitreloy 1) exhibits an exceptional glass forming ability (GFA) and thermal stability with respect to crystallization [1–3]. However, because of their inherent stability, metallic glasses undergo a large change during thermal treatment, the final step is crystallization. A lot of experiments (e.g. electrostatic levitation and calorimetric methods [4–9], small neutron angle scattering [3,10–13]) have shown that in this alloy, the primary crystallization is preceded by phase separation in the supercooled liquid region (SLR). In addition, structural relaxation is always observed, in this metallic glass as in any kind of glassy material [14]. Consequently, the evolution from the as-cast state to the full crystallized state is complex.

* Corresponding author. Tel.: +33-4 72 43 83 18; fax: +33-4 72 43 85 28.

E-mail address: jean-marc.pelletier@insa-lyon.fr (J.M. Pelletier).

This evolution can occur either during continuous heating at increasing or decreasing temperature (with a fixed heating or cooling rate), or during isothermal treatment. This second approach seems to be better, since the temperature influence can be isolated in a more appropriate way. As mentioned above, a lot of techniques have been used to investigate the microstructure evolution. Calorimetric methods is one of the most common, but only few data have been reported during isothermal treatments. Therefore, such measurements will be carried in the present work. In addition, is has been shown in previously reported papers [15–19] that electrical properties, and especially the thermoelectric power (TEP), are very sensitive to any microstructure evolution, e.g. short or long range ordering and precipitation in crystalline materials, structural relaxation or crystallization in amorphous alloys. Consequently, another purpose of this report is to determine the progressive destabilization of the $Zr_{41.2}$–$Ti_{13.8}$–$Cu_{12.5}$–Ni_{10}–$Be_{22.5}$ alloy by performing TEP measurements.

An other route to get detailed information on the microstructure evolution is to use mechanical spectroscopy. Indeed, measurements of the complex dynamic modulus can provide much information about atomic rearrangements and kinetics of atomic movements [20–22].

Finally, transmission electron microscopy is required to detect the onset of crystallization and the evolution of the particle size.

2. Experimental procedure

Ingots of amorphous materials, prepared by induction melting in controlled atmosphere and rapid quenching, have been supplied by Howmet Corp. (USA). Specimen were machined from plates ($400 \times 250 \times 3.3$ mm^3).

A differential scanning calorimetric apparatus (differential scanning calorimetry, DSC) (Perkin Elmer 7) was used between 200 and 550 °C in a purified argon atmosphere. Heating rate were in the range 1–60 °C/min.

TEP measurements were carried out at room temperature (293 K) after annealing in different conditions. The experimental set-up has been described elsewhere [15]. The TEP of the specimen was measured with reference to pure aluminum whose absolute TEP is known [23]. Since the interesting feature is the TEP evolution vs time and annealing temperature, only relative changes will be measured. The reference value corresponds to the as-cast specimen.

Structure of the material, examined by X-ray diffraction, using the Cu-Kα radiation, is amorphous in the as-cast condition.

Complex shear modulus G^* was measured under vacuum (10^{-3} Torr) from room temperature to 600 °C, between 10^{-4} and 1 Hz. Shear storage modulus G' and shear loss modulus G'' were determined either as a function of increasing or decreasing temperature (1–3 or 10 K/min) at fixed frequency or as a function of frequency at fixed temperature.

Samples for the TEM observation were prepared by dimpler polishing followed by ion beam milling. Conventional TEM observations were performed on a JEOL 200 CX microscope. A JEOL 2010F apparatus equipped with an energy dispersive X-ray spectroscopy (EDX) analyzer (Link-Isis Oxford) and a Gatan DigiPEELS Parallel spectrometer is used for high resolution TEM imaging and chemical nanoanalysis.

3. Experimental results

3.1. DSC results

In order to detect the temperature range in which a significant evolution of the material occurs, DSC experiments were first performed during heating with a fixed heating rate (10 °C/min). In agreement with results reported by various authors [4–9], DSC traces (Fig. 1) shows an endothermal heat effect due to the glass transition ($T_g = 363$ °C), followed by two exothermal heat effects. Hays et al. [6,8] attributed the first exothermic peak to phase separation and primary crystallization and the second one to a second crystallization (leading to a more stable crystalline phase).

Then, isothermal DSC experiments were carried out in a temperature range (350–430 °C) which corresponds, schematically, to the SLR. Fig. 2

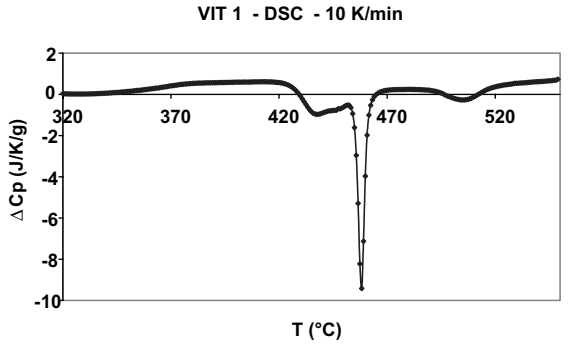

Fig. 1. DSC thermogram during continuous heating at 10 °C/min.

shows the relative evolution of the specific heat C_p vs time. Kinetics and magnitude of the variation are temperature dependent. Let us for instance describe the curve recorded at 410 °C, which exhibits a characteristic behaviour. This behaviour is manifested by a slight evolution during the first minutes of aging, followed by two distinct exothermal heat effects, similar to those obtained during continuous heating. Consequently, the existence of a preliminary evolution before the crystallization phenomenon is observed.

3.2. TEP measurements

3.2.1. Isothermal annealing

It is difficult to perform in situ TEP measurements during heating at high temperature. Therefore, specimen in the as-received condition were

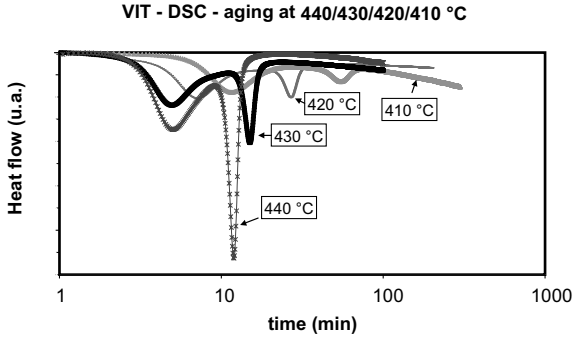

Fig. 2. DSC thermogram during annealing at various temperatures.

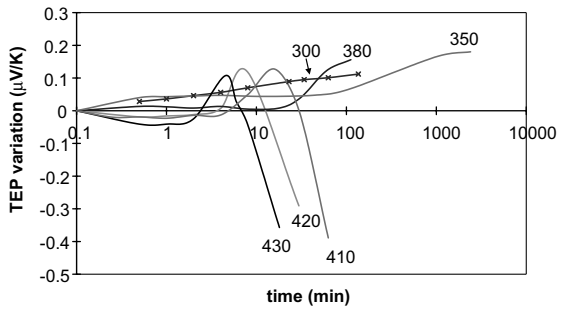

Fig. 3. Relative TEP vs annealing time at various temperatures.

isothermally treated at various temperatures T_A by immersion in a salt bath. It was verified, by comparison with some samples heated in evacuated tubes, that under the operating conditions, this procedure did not exert any disturbing influence (i.e. the same TEP values are obtained). Salt baths enable a very high heating rate to be used (only a few seconds are required to obtain the chosen temperature). Therefore, the initial stages of evolution can be investigated precisely. The results are shown in Fig. 3. The followings features are observed.

(i) In the initial stage, the TEP undergoes a slight change: an increase or a decrease, depending on the temperature. When the aging is carried out at $T_A > 390$ °C (approximate value), a decrease is observed, while an increase is induced by an aging at $T < 390$ °C. In addition, the magnitude of this effect increases as the difference $|T_A - 390\ °C|$ increases. Fig. 4 shows this initial evolution with expanded scaling.

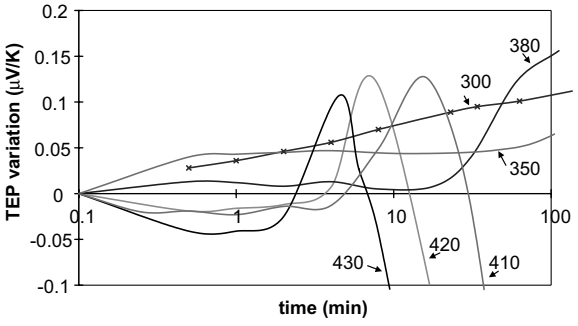

Fig. 4. Initial evolution of the relative TEP (expanded scaling of Fig. 3).

(ii) Then a large evolution in the TEP occurs. An increase is observed in the time range $t_0 < t_A < t_1$ (t_A: annealing time), followed by a rapid decrease for $t_A > t_1$.

Isothermal treatments were not prolonged, because of eventual oxidation in salt baths. The present results clearly show the high sensitivity of TEP to structural modifications.

As the curves are regular, the corresponding apparent activation energy E_A for these evolutions may be deduced by a conventional method, for instance the Kissinger–Boswell method [24, 25]. Results are as follows: $E_A(t_0) = 3.2$ eV and $E_A(t_1) = 3.8$ eV.

3.2.2. Existence of reversible phenomena

As mentioned above, the initial stage of the evolution of the alloy induces a variation in the TEP with a small magnitude, which depends on the isothermal aging temperature T_A. In order to determine the origin of these variations (reversible or irreversible), the following experiments have been conducted (Fig. 5):

(i) A first aging was carried out at a temperature T_{A1}, up to the beginning of stabilization at this temperature.
(ii) Then a further aging treatment was conducted at T_{A2} ($T_{A2} > T_{A1}$), to detect any structural evolution. Only short aging times are employed, in order to avoid any onset of crystallization in the next aging step (iii).
(iii) Finally, an other aging treatment was performed at T_{A1}.

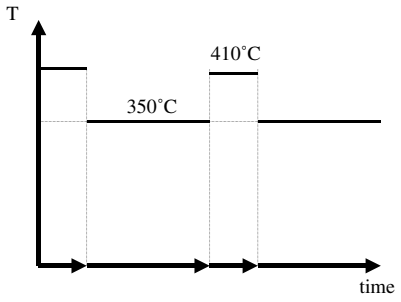

Fig. 5. Schematic representation of the heat treatment sequence conducted to determine the possible existence of reversible variations.

TEP was measured during the various stages (Fig. 6). 350 and 410 °C were retained for T_{A1} and T_{A2}, to allow significant variations with appropriated aging duration. The following points may be noticed:

- The initial aging at T_{A1}, which induces a TEP increase, do not prevent a further change at $T_{A2} = 410$ °C: TEP decreases and the final value is the same as that which would be obtained after a direct annealing at 410 °C.
- The second aging at $T_{A1} = 350$ °C induces the same variation as the first one. Magnitude and level are unchanged. Therefore, it can be concluded that the TEP evolution observed during the first stage of aging is reversible and so it is clearly demonstrated that the microstructure state corresponding to these preliminary stabilization values (before crystallization) reached at

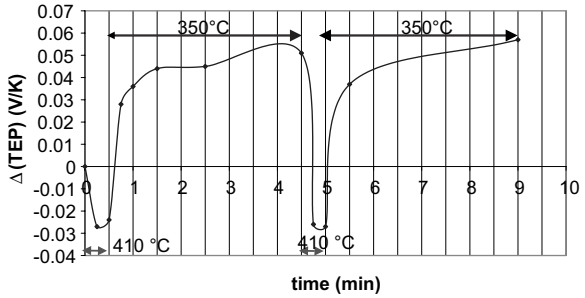

Fig. 6. Successive TEP variations observed during successive annealing treatments.

various temperatures are different. This reversible change could be due to short range chemical or topological ordering. In crystalline alloys, TEP variations associated to short range ordering modifications have been described using physical models [16]. However, in amorphous alloys, the physical origin of these variations is till an open question (see Section 4).

3.3. X-ray diffraction experiments

X-ray diffraction experiments have been performed at room temperature on a sample annealed at 410 °C during various times, as shown in Fig. 7. Characteristic times have been defined. The corresponding X-ray diffraction patterns have been recorded. The data for each annealing conditions are shifted along the intensity axis to enable a better comparison. In the as-cast specimen X-ray diffraction pattern reveals an amorphous state. Lines characteristic of crystalline phases commonly observed in Zr–Ti–Cu–Ni–Be alloys appear progressively. This growth can be associated to the TEP variations. Let us notice that after the first annealing (4 min at 410 °C), which corresponds to the end of the preliminary TEP evolution, X-ray diffraction pattern is very similar to that obtained in the as-cast condition.

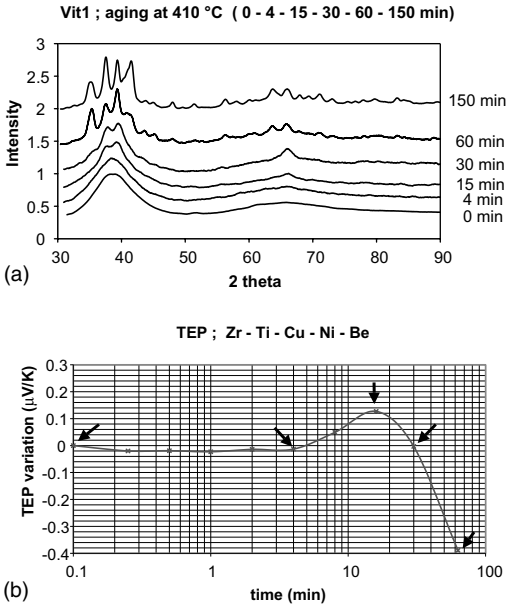

Fig. 7. (a) X-ray diffraction pattern in specimens annealed during various times at 410 °C. (b) These times corresponds to particular steps of microstructure evolution, as shown on the TEP curve relative to an annealing at 410 °C.

3.4. Influence of phase separation and crystallization on the dynamic shear elastic modulus

Fig. 8 shows the temperature dependence of the storage modulus G' when a constant frequency (0.3 Hz) and a constant heating rate (3 K/min) are used. G_u corresponds to the unrelaxed shear modulus. Evolution of G' with temperature occurs in several stages, in agreement with DSC results. Above a critical temperature T_α, a rapid decrease occurs, which is generally referred to the main relaxation (called also α relaxation) and is associated with the glass transition process. Subsequently, several steps of changes correspond to the multistage crystallization process of the supercooled liquid as shown on DSC curves. The α relaxation, or dynamic glass transition, is associated to large scale molecular movements which are considered to be hierarchically correlated, but can be related to the elementary molecular motion [20].

Fig. 9 shows the storage modulus evolution occurring during isothermal annealing at 410 °C, in addition with both TEP and C_p measurements performed in the same conditions. The different steps of crystallization induce an increase of the storage modulus. However, this evolution is not

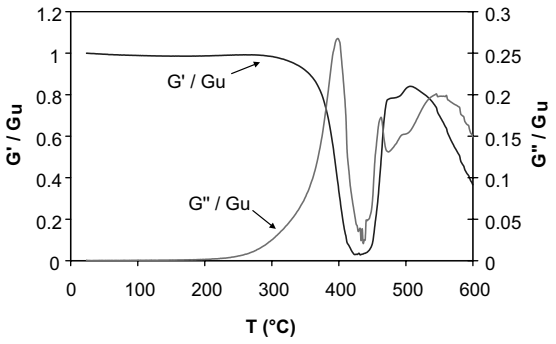

Fig. 8. Storage and loss elastic modulus versus temperature of the as-cast Vit1; frequency: 0.3 Hz; heating rate: 3 K/min.

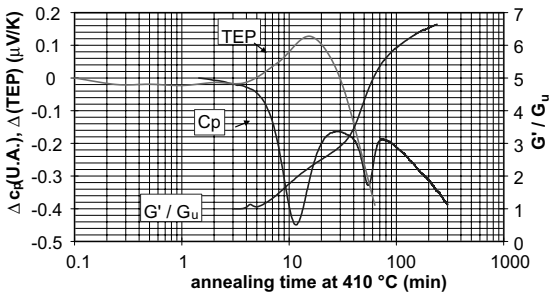

Fig. 9. Evolution of the elastic storage modulus during annealing at 410 °C.

regular. The first DSC peak is associated to a fairly limited shear modulus increase, while the second exothermic peak is related to a large elastic modulus increase (and a drastic TEP decrease). This increase of the rigidity of the material is due to the development of crystalline particles in the bulk amorphous matrix. Volume fraction of these particles increases with annealing time and, consequently, the role of the amorphous matrix is decreased. To evidence this effect, we performed continuous heating on preannealed samples. For comparison, we have also plotted in Fig. 10 the curves corresponding to the as-cast material and to a fully crystalline material achieved after a long annealing at 600 °C. This drastic change in G' is markedly reduced when the annealing time is increased, i.e. when the volume fraction of crystalline particles in increased. In addition, it is worth noting that both α relaxation and onset of further crystallization are shifted to higher temperatures.

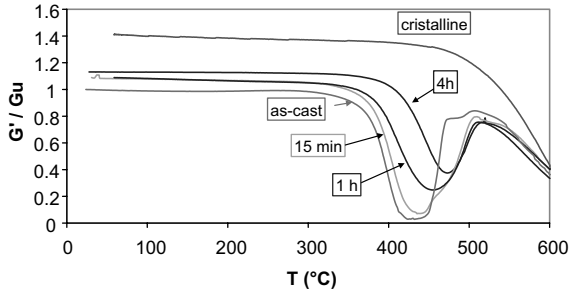

Fig. 10. Storage elastic modulus versus temperature of Vit1 after annealing at 410 °C during various time; frequency: 0.3 Hz; heating rate: 3 K/min.

Consequently, the thermal stability of the remaining amorphous matrix is higher than that of the initial amorphous phase before decomposition. Its glass transition is located at a higher temperature and it exhibits a larger SLR.

Even after a prolonged annealing at 410 °C (for instance 4 h), the main α relaxation is clearly observed. Behaviour of this composite material (amorphous matrix + nanocrystalline particles) is markedly determined by the amorphous matrix. Mechanical coupling between amorphous matrix and particles of the second phase seems to indicate that these crystalline particles do not form a rigid continuous network and are embedded in the remaining vitreous matrix. Nevertheless, existence of crystalline precipitates induces an elastic modulus increase. This increase is up to more than 40% when the transformation is fully achieved.

Fig. 11 shows a bright field image of the amorphous alloy after annealing at 410 °C during 7 min, as a typical example of the microstructure obtained upon heating. This microstructure produced by annealing consists of nanoparticles with average size of about 3 nm, which are embedded in the residual amorphous matrix. This average size depends on annealing time, as shown in Table 1. Annealing conditions were chosen so as to cor-

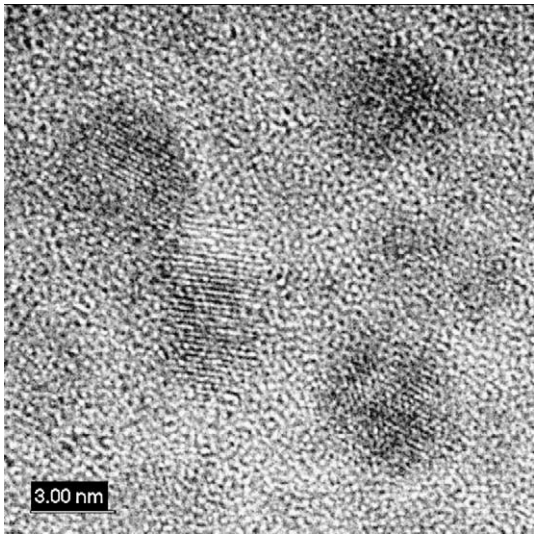

Fig. 11. TEM image of a nanocrystalline particles in the Vit1 annealed during 7 min at 410 °C.

Table 1
Average crystalline particle size after various annealing treatments

Annealing time at 410 °C (min)	5	7	9	25
Average size (nm)	0	3	6	22

respond to characteristic points in TEP or DSC curves. The onset of both TEP and C_p second evolution can be attributed to the formation of detectable nanocrystalline particles. These precipitates are randomly distributed in the matrix and their density seems to be large since the onset of their formation. A longer annealing time induces an increase of their average size rather than a modification of their density.

In order to quantify the volume fraction of nanocrystals in annealed samples, subsequent continuous heating were performed in the DSC apparatus. Thermograms are shown in Fig. 12. Usually, the volume fraction of the transformed material is estimated from the remaining crystallization enthalpy of the partially crystallized samples compared with the total crystallization enthalpy of the fully amorphous as-cast material. In the present conditions, this estimation is not so simple to perform. Indeed, as mentioned previously, devitrification occurs in two different steps and the relative magnitudes of these two exothermic peaks are affected by a prior annealing in a different way. Annealing effects affect both position and magnitude of the low temperature peak. In contrast, a short annealing modifies only the magnitude of the high temperature peak. Nevertheless, assuming that all these exothermic events are related to the crystallization process and that these various contributions can be added, a rough estimation of the volume fraction of nanocrystals formed during a given annealing can be deduced. Results are given in Table 2.

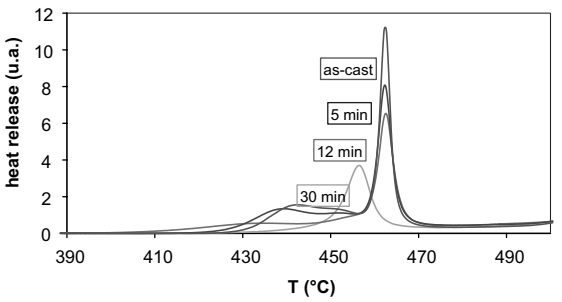

Fig. 12. Heat release during continuous heating at 10 K/min in samples annealed during various times at 410 °C.

Table 2
Volume fraction of crystalline particles after various annealing times at 410 °C (deduced from DSC experiments)

Annealing time at 410 °C (min)	0	5	12	30
Volume fraction of crystalline particles (%)	0	28	42	67

4. Discussion

From the various results (DSC, TEP, mechanical spectroscopy and TEM) performed either during continuous heating or during isothermal annealing, we confirm that the decomposition process taking place in the Vit1 occurs in different steps. In agreement with the small angle neutron scattering (SANS) data of Liu et al. [10,11] and Löffler et al. [12], it may be assumed that phase separation in the supercooled liquid precedes nucleation, resulting in two supercooled liquid phases with two different compositions. During this phase separation process, diffusion occurs, leading to a new short range order. This evolution is indicated by the first DSC peak, the limited storage modulus increase and the positive TEP increase. Let us mention that this evolution is partially reversible as indicated by the TEP measurements performed after short annealing at two different temperatures: 350 and 410 °C. Evolution induced at 350 °C is reverted by a further annealing at 410 °C, but is again observed during a subsequent heating at 350 °C and so on. TEM observations cannot reveal this evolution, probably due to the very small scale of these events.

These results are consistent with those reported by various authors, who reported that primary crystallization is preceded by phase separation in the SLR. The investigation of the composition fluctuations during phase separation using field ion microscopy with atom probe [12,13] presents

direct evidence that there exists an anti-correlation fluctuation of Be and Ti in the decomposition process, the decomposition involves mainly Be and Ti contents in the alloy. The large influence of the Be content on thermal stability and crystallization behaviour was underlined by various authors [12,26]. Liu [10] and Liu et al. [11] have shown using small angle neutron scattering that the initial decomposition in the SLR develops rapidly in the early stage, leaving a sluggish coarsening stage. The correlation function after different annealing times have been developed and roughly periodic modulated two supercooled liquid phase microstructure have been revealed. Wang et al. [27] have used electron diffraction intensity analysis to determine the reduced density function of the various elements, especially Zr and Be. They have shown that the decomposition has significant effect on the chemical and topological configuration of the amorphous alloy and that, at least, Be and Zr arrangements are largely rearranged after the phase separation and that the decomposed two amorphous phases have different short range order. All these data are consistent with our TEP measurements relative to reversible modification attributed to short range order which is temperature dependent. In addition, the results of small angle neutron scattering measurements conducted by Schneider et al. [3] indicated that the phase separation process shows many features of a spinodal decomposition [28], with a spinodal temperature of 398 °C. This critical temperature is close to the transition temperature of 390 °C observed in performing TEP measurements (let us notice that a more detailed investigation in this transition range is required to give a precise value of this parameter).

Then, during a second step of annealing, a second DSC peak appears at higher temperature during continuous heating or after a longer annealing time during isothermal annealing. Crystalline particles are clearly observed on TEM micrograph, in spite of their small size (only a few nanometers). This onset of crystallization results in a large increase of the elastic shear modulus and a negative variation of TEP. X-ray diffraction reveals also the appearance of this new crystalline particles. Since phase separation initiates crystallization, one obtains a crystalline phase embedded in a decomposed amorphous phase which do not form a continuous network of rigid particles. Consequently, the mechanical behaviour of this partly decomposed metallic glass is typical of a material in which the hard and rigid particles (i.e. the crystalline particles) are dispersed in a vitreous matrix and in which no percolation occurs. Indeed, the elastic modulus evolution versus the measurement temperature still exhibits the main α relaxation characteristic of all amorphous materials (polymers, oxide glasses, molecular glasses). The existence of a second crystalline phase reduces the magnitude of this relaxation, but do not completely suppress this phenomenon. The isolated nanocrystals do not significantly influence the elastic features of this composite material and therefore the overall shear modulus could not probably be expressed by a single volume fraction rule. In order to get a better description of the elastic properties of this semicrystalline material, more sophisticated models should be developed (see for instance [20,22]). The stress level involved during mechanical spectroscopy tests is very low, much smaller than the yield strength and consequently, nanocrystals cannot be arranged during loading and contribute significantly to the deformation by forming, for instance, alignments in the loading direction. This result agrees with those reported by other authors, who observed that the partially nanocrsytalline two-phase samples produced by annealing exhibit significantly reduced ductility. The elastic behaviour is almost identical to that of the fully amorphous alloy, at least when the volume fraction of the crystalline second phase is lower than about 40–50%.

5. Conclusion

The evolution during an isothermal annealing, of the microstructure in a bulk metallic glass (Vitreloy 1) was investigated as a function of time and temperature, in the SLR. Crystallization is preceded by a phase separation phenomenon, which induces only a slight heat capacity variation, but a significant TEP change. This TEP change can be reverted by annealing at a different temperature.

For instance, the evolution observed during annealing at 350 °C is modified by a further annealing at 410 °C but takes place again during a final annealing at 350 °C. A transition temperature is observed, which corresponds to a change of the sign in the TEP evolution. This temperature could be associated to the spinodal temperature determined by various authors using, for instance, small angle neutron scattering. Then, a second stage corresponds to the onset of crystallization, an irreversible phenomenon. Large exothermic heat effects and TEP variations are associated to this crystallization of the metastable supercooled liquid.

References

[1] A. Peker, W.L. Johnson, Appl. Phys. Lett. 63 (1993) 2342.
[2] W.L. Johnson, Mater. Sci. Forum 225–227 (1996) 35.
[3] S. Schneider, W.L. Johnson, P. Thiyagarajan, Appl. Phys. Lett. 68 (1996) 493.
[4] Y.J. Kim, R. Busch, W.L. Johnson, A.J. Rubson, W.K. Rhim, Appl. Phys. Lett. 65 (1994) 2136.
[5] T.A. Waniuck, R. Busch, A. Masuhr, W.L. Johnson, Acta Mater. 46 (1998) 5229.
[6] C.C. Hays, C.P. Kim, W.L. Johnson, Appl. Phys. Lett. 75 (1999) 1089.
[7] W.H. Wang, H.Y. Baï, Appl. Phys. Lett. 84 (1998) 5961.
[8] C.C. Hays, C.P. Kim, W.L. Johnson, Mater. Sci. Forum 312–314 (1999) 469.
[9] B. Spriano, C. Antonione, R. Doglione, L. Battezzati, S. Cardoso, J.C. Soares, M.F. Da Silva, Philos. Mag. 76 (1997) 529.
[10] J.M. Liu, Mater. Sci. Eng. A222 (1997) 182.
[11] J.M. Liu, A. Wiedenmann, U. Gerold, U. Keiderling, H. Wollenberger, Phys. Stat. Sol. b 199 (1997) 379.
[12] J.F. Löffler, W.L. Johnson, Appl. Phys. Lett. 76 (2000) 3394.
[13] M.P. Macht, N. Wanderka, A. Wiedenmann, H. Wollenberger, Q. Wei, H. Fecht, S.G. Klose, Mater. Sci. Forum 225–227 (1996) 65.
[14] A.L. Greer, Nature 366 (1993) 6453.
[15] J.M. Pelletier, R. Borrelly, E. Pernoux, Phys. Stat. Sol. A 39 (1977) 525.
[16] G. Vigier, J.M. Pelletier, Acta Metall. 30 (1982) 1851.
[17] J.M. Pelletier, G. Vigier, J. Merlin, P. Merle, F. Fouquet, R. Borrelly, Acta Metall. 32 (1984) 1069.
[18] J.M. Pelletier, F. Fouquet, J. Hillairet, Phys. Stat. Sol. a 93 (1986) 703.
[19] J.M. Pelletier, F. Fouquet, S. Bouras, Mater. Sci. Eng. 77 (1986) 175.
[20] J. Perez, in: A.A. Balkem (Ed.), Physics and Mechanics of Amorphous Polymers, Brookfield, Rotterdam, 1998.
[21] A.S. Nowick, B.S. Berry, Anelastic Relaxation in Crystalline Solids, Academic Press, New York, 1972.
[22] J.D. Ferry, Viscoelastic Properties of Polymers, John Wiley, New York, 1990.
[23] R.B. Roberts, Philos. Mag. 36 (1997) 9.
[24] H.E. Kissinger, Anal. Chem. 29 (1957) 1702.
[25] P.G. Boswell, J. Therm. Anal. 18 (1980) 353.
[26] W.H. Wang, Q. Wei, S. Friedrich, J. Mater. Sci. 35 (2000) 2291.
[27] W.H. Wang, Q. Wei, S. Friedrich, M. Macht, N. Wanderka, H. Wollenberger, Appl. Phys. Lett. 7 (1997) 1053.
[28] J.W. Cahn, Acta Metall. 9 (1961) 795.